Natural Hazards
https://doi.org/10.1007/s11069-024-06498-0

ORIGINAL PAPER

Force coefficients for modelling the drift of a victim of river drowning

C. Delhez[1] · T. Andrianne[2] · S. Erpicum[1] · N. Riviere[3] · P. Hallot[4] · M. Pirotton[1] · P. Archambeau[1] · B. Dewals[1]

Received: 18 October 2023 / Accepted: 7 February 2024

Abstract

The global annual death toll due to drowning is of the order of 10^5. Rescue and search operations in urban rivers show a low rate of success. Operational computational drift models have been developed for marine environments but not for the case of river drowning. In the latter case, no scale separation occurs between the body and flow length scales. To model them, three hydrodynamic force coefficients of representative bodies, such as drag, side and lift coefficients, are needed. So far, their value was not characterized for the typical positioning of the body of a drowning victim. In this work, we used full-scale laboratory experiments to identify the range of value of these hydrodynamic coefficients based on 249 tests conducted in a wind tunnel. Observations in the air can be transferred to water environment thanks to flow similarity. For the typical body positioning of a drowning victim, the drag coefficient was found to vary in the range 0.5–1.2. Changing the yaw angle of the body, induces variations in the drag coefficient by about 50%. Considering loose clothes instead of tight clothes leads to an increase in the drag coefficient by about 30%, whereas adding a backpack has a limited influence (less than 5%). With the available experimental setup, it has been difficult to detect distinctive patterns and trends for the side and lift coefficients. This study is part of a multidisciplinary effort for developing scientific knowledge and technologies contributing to a reduction of drowning-induced fatalities in rivers.

Keywords Drowning · River · Wind tunnel · Drag coefficient · Lift coefficient · Side coefficient

✉ C. Delhez
clement.delhez@uliege.be

[1] Hydraulics in Environmental and Civil Engineering (HECE), Research Unit Urban and Environmental Engineering (UEE), University of Liège, 4000 Liège, Belgium

[2] Aerospace and Mechanical Engineering, University of Liège, 4000 Liège, Belgium

[3] Univ Lyon, INSA Lyon, Ecole Centrale de Lyon, Université Claude Bernard Lyon I, CNRS, LMFA, UMR 5509, 20 Avenue Albert Einstein, 69621 Villeurbanne, France

[4] DIVA, Art Archaeology Heritage, University of Liege, 4020 Liege, Belgium

Published online: 24 February 2024

1 Introduction

1.1 Context

Worldwide, unintentional drowning claims a total of nearly 400,000 lives every year (WHO 2014), and drowning is among the main causes of death of young people (Ung et al. 2019). Climate change increases the risk of drowning, as hydro-meteorological extremes are becoming more frequent (Parks et al. 2020). Both floods and heatwaves cause drowning accidents. In urban rivers, heatwaves trigger a rise in (unauthorized) bathing activities, hence also in accidental drowning. Recent urban planning policies promoting the use of riverbanks for their amenities (cooler atmosphere, scenic views, safe paths for walking and cycling) make it particularly timely to address the issue of drowning in urban rivers. Compared to drowning in swimming pools or at the seaside, the chance of survival after river drowning is two to three times lower (Byard 2017).

Causes of drowning in urban rivers are numerous, including bathing, traffic accidents, influence of drugs or alcohol, and suicidal or criminal acts (e.g., Kringsholm et al. 2001). Reducing the number of fatalities due to drowning requires a holistic approach combining epidemiological studies, prevention measures (education, rising risk awareness, fences, bathing surveillance or bans), improved resuscitation techniques and medical treatment (Bierens 2006), as well as a better preparation for rescue and search operations. Compared to the case of lakes or pools, body search operations in urban rivers are particularly complex due to relatively high flow velocity and low visibility, as well as the presence of subsurface vortices created by obstacles (Strom et al. 2017), such as bridge piers and weirs, or by ship motion. Technologies such as sonars perform poorly in urban rivers due to debris lying on the bottom, which make it harder to discern a body shape (Blondel 2014; Ruffell et al. 2017). So far, search operations in urban rivers have not been guided by existing modelling technologies enabling accurate simulation of the flow field in a river. Though, such models have the potential to inform more targeted rescue and search operations, and to provide valuable information for forensic analyses (Carniel et al. 2002; Ruffell et al. 2017; Mateus et al. 2020). So far, modelling studies on drowning in rivers focused on the incipient motion of human bodies, which may result from toppling or sliding (Jonkman and Penning-Rowsell 2008). Such studies did not extend to modelling the victim's trajectory in water.

1.2 Background

To the best of the authors 'knowledge, only a single modelling study investigated the drift of human bodies in a real river. Gonzalez et al. (2022) combined an Eulerian flow model of La Miel river in Colombia (grid size of the order of 1 m × 1 m) with a Lagrangian drift model. Though they pointed at regions where synthetic floats tend to accumulate, they mostly presented hydrodynamic results and did provide an in-depth analysis of flow-body interactions in rivers. They are primarily interested in the drift of human remains in the context of an armed conflict, and not to accidental drowning. In contrast, a range of computational studies addressed the drift of a victim of drowning at sea or ocean. They are summarized in Table 1. Delhez et al. (2023) tested a similar model but only in highly idealized flow conditions.

Table 1 Existing computational models of the drift of victims of drowning in coastal waters

	Grid size	Time step	Considered drivers of body drift			
			Current	Waves	Wind	Body inertia
Carniel et al. (2002)	1 km	12 h	✓	✓	✓	No
Breivik and Allen (2008)	4 km	6 h	✓	(✓)[a]	✓	No
Mateus et al. (2015)	6.5 km	1 h	✓			No
Gunduz (2017)	4 km	Not specified	✓			No
Ličer et al. (2020)	1 km	12 min	✓	(✓)[a]	✓	No
Hart-Davis and Backeberg (2023)	9.2 km	1 h	✓	(✓)[a]	✓	No
Tu et al. (2021), Wu et al. (2023)	N/A[b]	10 min	✓		✓	No

[a]The brackets indicate that the effect of waves is not explicitly reproduced in the Lagrangian model because it is considered as already incorporated in the empirical leeway coefficients used for modelling wind effects

[b]Tu et al. (2021) and Wu et al. (2023) used field measurements of flow and wind velocity (instead of Eulerian models) to force their Lagrangian body drift computations

Carniel et al. (2002) used a computational model to confirm the plausibility of the drift of a floating body over 300 km in two weeks in the Mediterranean sea. Ocean currents and waves were simulated by an Eulerian ocean circulation model forced by regional atmospheric models. The grid resolution was 10 km and the time step 12 h. The outcomes of the ocean circulation model were used to drive a Lagrangian model of the drifting body, accounting for the effects of currents, waves (Stokes drift) and wind. A random walk component was included to reproduce the influence of fluctuations not resolved by the Eulerian model.

Breivik and Allen (2008) combined oceanic and atmospheric models with a drift model for a range of objects, including human bodies. In the drift model, current and wind effects were explicitly considered. The Stokes drift (i.e., effect of waves) was not modelled explicitly because it is considered as already incorporated in leeway empirical coefficients used for parametrizing wind forcing. A Bayesian stochastic framework was adopted to account for uncertainties in the forcing fields (wind and current), body characteristics and initial position. The model outcome is a time-dependent probability density function of the object location.

Mateus et al. (2015) studied the case of a body drifted over only 2 km in 8.6 days in a coastal area of Portugal, as previously reported by Mateus et al. (2013). The flow field was simulated by an ocean circulation model forced by wind, tide, and discharge of a river, whereas the body motion was computed with a Lagrangian drift model forced by currents only. The same modelling approach was used by Gunduz (2017) to investigate an accident in which victims drifted over 100 km in seven days.

More recently, similar modelling frameworks were presented by Ličer et al. (2020) and by Hart-Davis and Backeberg (2023). For the same reasons as Breivik and Allen (2008), both studies explicitly considered the influence of currents and wind in the Lagrangian drift model but not the effect of waves. Tu et al. (2021) and Wu et al. (2023) also applied a Lagrangian model for simulating the drift of a human body at sea, but their model was forced by field observations of current and wind velocity.

All computational studies reported in Table 1 analysed the drift of bodies in sea or ocean environments, which differs from the case of river drowning in two key aspects. First, all these studies considered the body as a passive float. This assumption is reasonable in sea or

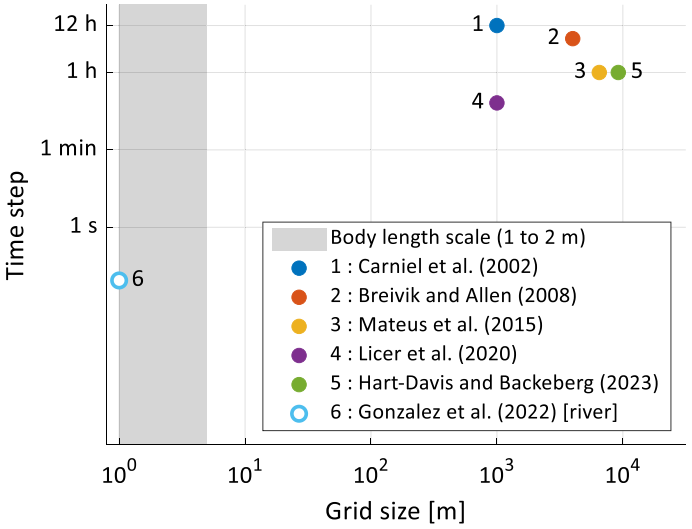

Fig. 1 Characteristic time- and length-scales in sea and ocean environments compared to the body size and the corresponding scales in rivers

ocean environments because the body length scale (of the order of 1 to 2 m) is way smaller compared to the flow lengths scales. This is illustrated in Fig. 1, which highlights that the grid size (considered as a proxy for the resolved flow lengths scales) in the models listed in Table 1 exceed the body length scale by three to four orders of magnitude. This length scale separation, together with the large considered time scales (vertical axis in Fig. 1 and Table 1), supports the idealization of the body as a passive float, for which the duration of body acceleration phases is negligible compared to time resolution of the computations (Breivik and Allen 2008).

In contrast, in urban rivers, the characteristic length scales of the flow are much smaller due the topographic variability induced by features such as bridge piers, hydraulic structures, riverbanks, meanders. This leads to variations in velocity direction and magnitude over comparatively small distances and durations. In such conditions, assuming that the body velocity remains equal to the flow velocity does not hold true (Breivik and Allen 2008; Ghaffarian et al. 2020). Indeed, due to body inertia, the velocity changes induce a non-zero relative velocity between the drifted body and the river flow. Hence, the drag and, to a lesser extent, the side forces induced by the relative motion between the body and the flow need to be considered, unlike for large scale modelling in sea or ocean environments (Table 1). This requires the knowledge of the corresponding hydrodynamic coefficients (drag and side coefficients).

Second, all previous models assumed a positively-buoyant body, so that only a 2D horizontal body motion was reproduced. Since freshwater has a lower density than sea water and lifejackets are less often worn in the case of river drowning, the body of a victim of river drowning may be either positively or negatively buoyant (Donoghue and Minnigerode 1977; Martlin et al. 2023). As the drift velocity differs substantially whether the body is at the surface or close to the bottom, it is of most importance to predict the body vertical motion. This motion over the flow depth is influenced by several parameters relatively intricate to predict (Martlin et al. 2023), such as body morphology (Modell and Davis

1969; Gallagher et al. 1996; Barwood et al. 2011; Laurent et al. 2013; Van Hoyweghen et al. 2015), presence of air or water in the lungs (Modell and Davis 1969; Gallagher et al. 1996; Barwood et al. 2011; Laurent et al. 2013; Van Hoyweghen et al. 2015), amount of water swallowed by the victim (Modell and Davis 1969), type of clothes (Modell and Davis 1969; Gallagher et al. 1996; Barwood et al. 2011; Laurent et al. 2013; Van Hoyweghen et al. 2015), accessories such as a backpack. Since a human body in water may be close to neutrally buoyant, even a relatively small lift force induced by the flow may change the direction of the net force along the vertical direction. Therefore, estimating the lift coefficient of the body of a drowning victim is of practical importance.

1.3 Objectives

No study so far focused on the determination of hydrodynamic coefficients, such as drag, side and lift coefficients, for a human body in conditions representative of a victim of river drowning. The forces resulting from body-flow interactions depend on the body positioning. Field observations suggest a typical body positioning for victims of drowning, irrespective of whether the body is close to the surface, in sinking phase, or resurfacing (Fig. 2): as long as the body is not in contact with the bottom, unconscious bodies are mainly found face downwards, limbs hanging down (Blanco Pampín and López-Abajo Rodríguez 2001; Lunetta et al. 2014). This positioning results from the relative value of the limbs and torso densities. Regardless of the precise drowning circumstances, a certain quantity of air remains in the lungs, giving them a lower density than the rest of the body. Besides, after the heart stops, the blood pressure drops, and blood accumulates in the lower parts of the body (i.e., hands and feet in this case), consistently with the *livor mortis* phenomenon (Amendt et al. 2004). In the case of a resurfacing body, putrefaction gases cause inflation of the abdomen (Laurent et al. 2013), leading to a similar positioning as in the sinking phase. The case of a body in contact with the bottom is out of the scope of the present study.

In previous studies analysing the drag coefficient, and to a lesser extent the side and lift coefficients, of a human body, the body positioning differed from the typical one of a drowning victim, as they focused on the cases of swimming (Bixler et al. 2007; Marinho et al. 2009, 2011, 2012; Zamparo et al. 2009; Mantha et al. 2014), ice skating (Ingen

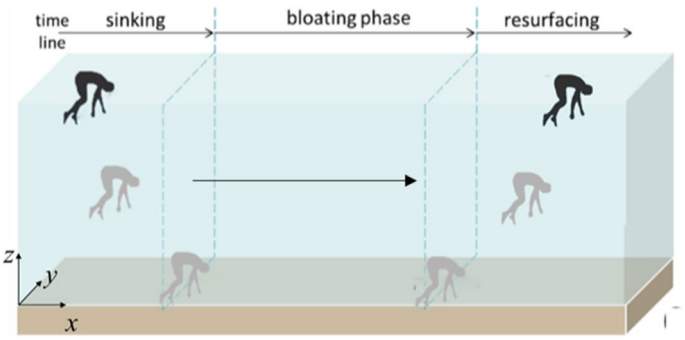

Fig. 2 Sketch of typical body positioning of a drowning victim. The body trajectory generally follows three stages: body sinking, body bloating (due to the generation of gases as a results of body decomposition) usually on the bottom, and body resurfacing. Adapted from Mateus et al. (2013)

Schenau 1982), ski jumping (Müller 2009; Wolfsperger et al. 2021), speed skiing (Barelle et al. 2004), cycling (García-López et al. 2008), and standing, sitting or supine positions (Schmitt 1954) but not for the case of a drowning position.

In this study, we undertook laboratory experiments with a full-scale dummy to determine the drag, side, and lift coefficients of a human body in a typical position of river drowning (face down, limbs hanging down). The body yaw angle (i.e., the rotation of the body around the vertical axis) was systematically varied (Fig. 3). For the sake of assessing the influence of the body position, tests with a lying body were also undertaken. The experiments were conducted in a wind tunnel, which offers more flexibility and an easier access to the body than a towing tank or a hydraulic flume. The results may be transferred to the case of a body in water using similarity rules. The influence of clothes and of presence of accessories, such as a backpack, were also investigated.

Section 2 presents the experimental setup, the test program, and the measurement techniques. The results are detailed in Sect. 3, while they are compared to previous studies in Sect. 4. Concluding remarks are formulated in Sect. 5.

2 Materials and methods

When a body is immerged in a fluid with a non-zero relative velocity, friction stresses and pressure differences around the body add up so that a resulting force is induced by the flow on the body (Hoerner 1965; Cook 2007). As sketched in Fig. 3, this force is generally separated into three components, referred to as drag (F_D), side (F_S) and lift (F_L) forces, which are respectively aligned along the direction of the approaching flow, horizontally in the plane normal to the approaching flow, and vertically in the same plane (Cook 2007). Each of these three force components is generally estimated as a function of the fluid density, the body frontal area and the square of the relative velocity, using corresponding hydrodynamic coefficients called drag (C_D), side (C_S) and lift (C_L) coefficients (Cook 2007). These coefficients are Reynolds-dependent, and they vary with the body shape, positioning and directionality. Here, the value of these coefficients was experimentally determined for a human body in a typical position of a drowning victim.

In this section, the wind tunnel and the dummy used for the laboratory tests are presented (Sects. 2.1 and 2.2). The considered flow scenarios are introduced in Sect. 2.3. In Sect. 2.4, the hydrodynamic coefficients are described, as well as the method used to obtain each of them from the experimental measurements. Finally, the test program is detailed in Sect. 2.5.

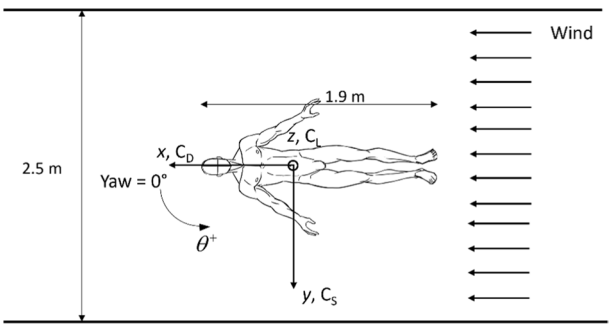

Fig. 3 Sketch of the wind tunnel setup, with the dummy in lying position and a yaw angle $\theta = 0°$

2.1 Experimental setup

The experimental tests were conducted in the wind tunnel laboratory of University of Liege (Belgium). For technical reasons, a wind tunnel was preferred over a towing tank or a current flume. The wind tunnel enables rapid data acquisition and easy access to the test area, making it simple to systematically vary the dummy configuration (e.g., covering a high number of different yaw angles, changing dummy positioning and/or clothes). Preliminary tests were performed in a towing tank (100 m in length, 6 m in width, and 4 m in depth); but repeatedly adjusting the dummy position and test configuration proved more challenging due to the underwater location of the dummy and attachment system. Since a wind tunnel was utilized, the influence of a river free surface on the results should be investigated in a subsequent step of the research.

The cross-section of the wind tunnel is 2.5 m wide and 1.8 m high (Fig. 3). The wind is blown along the wind tunnel longitudinal direction, referred to as streamwise direction x, positive in the wind direction. The lateral and vertical directions to the flow direction are labelled y and z, respectively (Fig. 3). In the present tests, the wind velocity U_x ranges from 3.2 to 6.5 m/s with a turbulence intensity of 0.5%. The facility is equipped with a load balance (Omega 160 ATI sensor) enabling force and torque measurements in the three directions. The load balance has a sensing range of 1000 N in the streamwise and lateral directions and 2500 N in the vertical direction. All sensing ranges are 120 Nm for the torques. The resolution of the sensors on each force is 0.25 N, of 0.025 Nm for the torques around direction x and y and of 0.0125 Nm for the torque around the vertical axis. Data were acquired at a frequency of 200 Hz. Based on a convergence analysis, the mean and standard deviation of each measured time series were computed, and the sampling time was set to 15 s (Figures S1 to S3 in Supplement). This sampling time is long enough to allow each of the measured component to converge in each configuration except for the force in the vertical direction. However, the average of this force is comparable to the resolution of the sensor in many configurations, so that these measurements were mostly discarded from the analyses.

A full-scale dummy was selected instead of a reduced-scale dummy to avoid issues related to geometric scaling of the test results, and to ensure that the measured forces can be reliably captured by the sensors. Indeed, using a reduced scale dummy would have led to considerably smaller forces, while even in the present tests some of the forces (particularly the lift component) are already relatively small compared to the sensors resolution (Figure S6 in Supplement).

The full-scale dummy used in the tests is an adjusted version of the Rescue Randy 9000 manufactured by 3B Scientific (Fig. 4). It is made of rugged polyethylene. The dummy represents a male adult, 1.9 m tall, with a shoulder width of 0.54 m, arms of 0.77 m in length, 0.93 m-long legs and a body surface area of 2.46 m^2. Without clothes nor accessories, the dummy weights 30 kg. The dummy has joints, equipped with connecting screws, which give access to a wide variety of limbs positioning. Using tailored 3D-printed interlocking parts (Figure S7 in Supplement), the joints have been modified to enable firmly fixing the position of each ball joint to ensure enough rigidity for wind velocity up to 6.5 m/s. In all configurations, limbs and head are at least 15 cm away from walls and their development of boundary layer.

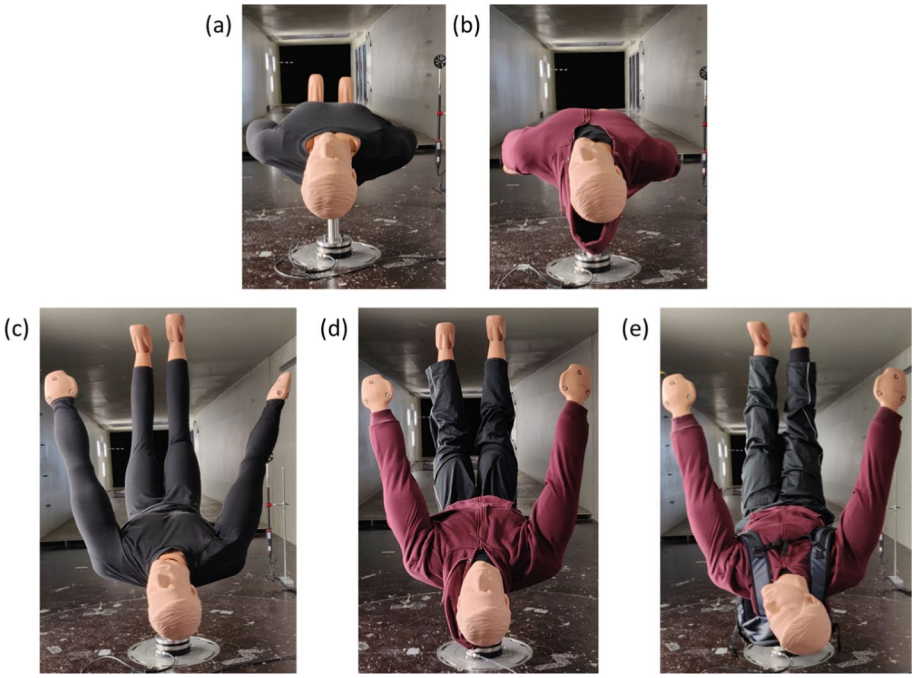

Fig. 4 Positions and types of clothes of the dummy (represented with wind coming from the background and a yaw angle of 0°): **a**, **b** lying position, **c**, **d**, **e** drowned position. **a**, **c** tight clothes, **b**, **d**, **e** loose clothes. **e** body wearing a backpack

2.2 Dummy positioning

In the experiments, two distinct dummy positions were tested. First, for the sake of comparison with existing measurements, the body was set lying with arms alongside the trunk and face up (Fig. 4a, b). The second position mimics the typical drowning positioning, as introduced in Sect. 1.3. This typical position of a drowning victim is mostly described in qualitative terms in literature and limited geometric details are available on the body positioning (Blanco and Lopez-Abajo, 2001; Lunetta et al. 2014). This prompted us to make plausible assumptions on the relative positioning of the torso, limbs, and head. In the conducted experiments, an angle of 75° was considered between the torso and the arms, and between the pelvis and the legs. The limbs were kept straight due to a lack of information on the degree of bending in actual cases. For technical reasons, the torso was placed horizontally in the wind tunnel and the limbs formed an angle of 15° with the vertical (Figure S8 in Supplement). In the wind tunnel, the dummy was positioned upside down (i.e., head facing up) compared to the body position typically observed in the field when a victim of drowning is found (i.e., head facing down). This choice does not affect the results. It was made to reduce the length of the measurement sting and keep parasitic moments in the measurements at a minimum. Nonetheless, for each considered wind velocity, tests were also conducted without the dummy for estimating the forces induced by the flow on the measurement arm, and correct for them (Sect. 2.4).

For each body positioning, the body yaw angle (noted θ) was systematically varied. This angle is defined equal to 0 when the spine is aligned with the main flow direction and the head is located downwind (Fig. 3). The yaw angle is positive in the counter-clockwise direction. Thirty different values of the body yaw angle were tested, in the range from 0° to 345°.

The dummy was dressed in either tight or loose clothes (Fig. 4). The former aim at representing a victim of a river bathing accident (i.e., naked or wearing a swimming suit), while still hiding the screws present at the dummy joints (Figure S9 in Supplement) which would otherwise bias the measurements. The loose clothing was used to represent more standard clothing of a drowning victim. In some tests, an empty backpack was added to appreciate the influence of such accessories (Fig. 4e).

2.3 Flow scenarios

In the wind tunnel, experiments could be conducted for wind velocity ranging from $U_x = 3.2$ m/s up to $U_x = 6.5$ m/s. Below 3.2 m/s, the sensitivity of the sensors did not allow retrieving a stable signal due to the low values of forces. Above 6.5 m/s, unacceptable vibrations of the dummy limbs were detected. Tests were conducted for the minimum value $U_x = 3.2$ m/s, the maximum one, $U_x = 6.5$ m/s, and an intermediate one, $U_x = 4.5$ m/s (Table 2).

During the tests, the air temperature was 9.8 °C and the atmospheric pressure was 100,100 Pa. This leads to a value of $\nu = 1.4 \times 10^{-5}$ m^2/s for the kinematic viscosity of air. Considering the body height as a characteristic length ($L = 1.9$ m, irrespective of the dummy positioning) like Bixler et al. (2007), Marinho et al. (2009) and Marinho et al. (2011), the Reynolds number $\mathrm{Re} = U_x\, L \,/\, \nu$can be evaluated for each considered wind velocity (Table 2). In the tests, the Reynolds number ranges between 4.3×10^5 and 8.8×10^5. From the value of the kinematic viscosity of water ($\nu = 1.007 \times 10^{-6}$ m^2/s), we may infer that the hydrodynamic coefficients determined from the tests conducted in the wind tunnel are comparable to those that would be obtained with the dummy immerged in a water flow with a relative velocity ranging between 0.23 and 0.46 m/s (Table 2). Although narrow, this range of relative velocity between the body and the flow is plausible. Besides, Reynolds numbers of the order of 10^5 correspond to a turbulent regime, in which the hydrodynamic coefficients, particularly the drag coefficient, vary little with the Reynolds number. Indeed, preliminary tests have revealed no drag crisis for Reynolds numbers in the range from 2.5×10^5 to 1.6×10^6.

Table 2 Tested wind velocities, Reynolds numbers and corresponding water velocities, if the same Reynolds number is assumed

Wind velocity (m/s)	3.2	4.5	6.5
Reynolds number (−)	4.3×10^5	6.1×10^5	8.8×10^5
Water velocity (m/s)	0.23	0.32	0.46

2.4 Determination of hydrodynamic coefficients

In each experimental test, the three components of the fluid-induced force were measured. They are referred to F_D, F_S and F_L. They are respectively aligned along the x, y and z reference axes (Fig. 3). The value of the torques along these three reference directions were also measured in each test. They are referred to T_x, T_y and T_z. These quantities are also referred to as moments (Tropea et al. 2007; Anderson 2011). Consistently with Sect. 2.1, each of these quantities was measured over a duration of 15 s and time-averaged. The forces and torques acting on the measurement arm alone were subtracted from the respective quantities to obtain the aerodynamic loading of the body only.

It is customary to relate the three force components to the square of the relative approach velocity U, the fluid density ρ the body frontal area A and non-dimensional coefficients, as follows:

$$F_D = \frac{1}{2}\rho\, C_D A U^2 \quad F_S = \frac{1}{2}\rho\, C_S A U^2 \text{ and } F_L = \frac{1}{2}\rho\, C_L A U^2 \tag{1}$$

where C_D, C_S and C_L are the drag, side and lift coefficients, respectively. In the experimental conditions, air density was 1.23 kg/m^3.

In Sect. 3, the experimental results are displayed in two different forms. On the one hand, we show the value of the products of the respective hydrodynamic coefficients and the corresponding frontal area:

$$C_D A = \frac{2F_D}{\rho\, U^2} \quad C_S A = \frac{2F_S}{\rho\, U^2} \text{ and } C_L A = \frac{2F_L}{\rho\, U^2} \tag{2}$$

The obtained quantities, $C_D\, A$, $C_S\, A$ and $C_L\, A$, are referred to as drag, side and lift areas, respectively. They offer the advantage of being independent of the evaluation of a frontal area, which is intricate as this area is strongly influenced by the body positioning, yaw angle, clothes and their interaction with moving air/water (swelling). This approach also avoids the selection of a particular reference area (e.g., kept unchanged when the yaw angle is varied), which would inevitably be somehow arbitrary.

It is common in sport aerodynamics to compare the aerodynamic effects in various positions of a given body (Blocken et al. 2018; Mannion et al. 2019; Wolfsperger et al. 2021). As such, the drag, side, and lift areas measured for one body do not apply for a body of similar geometry but at another scale. It is possible to scale these areas by dividing them by a reference area, independent of the yaw angle, of the body considered in the experiments and multiplying by the corresponding area of the body of interest. The obtained coefficients will experience the same variations as the force areas, but with values that depend on the reference area chosen, which could be the body surface area (Mosteller 1987; Du Bois and Du Bois 1989; Tikuisis et al. 2001; Yu et al. 2010).

We also evaluated the standard non-dimensional coefficients C_D, C_S and C_L, defined as follows:

$$C_D = \frac{2F_D}{\rho\, A\, U^2} \quad C_S = \frac{2F_S}{\rho\, A\, U^2} \quad \text{and} \quad C_L = \frac{2F_L}{\rho\, A\, U^2} \tag{3}$$

This requires an estimation of the body frontal area, for each body positioning and each considered yaw angle. To achieve this, a 3D digital model of the dummy was created based on a LIDAR scan. The obtained frontal areas for both body positions and

tight clothes are depicted in Fig. 5. For both positions, a periodicity can be observed in the variation of the frontal areas with the yaw angle. Frontal areas for the drowned position exhibit additionally local minima corresponding to yaw angles for which one limb hides another.

In the case of loose clothes, the frontal area is expected to be slightly larger irrespective of the body position and yaw angle. However, frontal areas with loose clothes could not be reliably measured due to the deformable nature of such clothes. Loose clothes are prone to catching the wind/water flow and can therefore inflate, increasing the frontal area. Such effects cannot be reproduced during a LIDAR scan of the dummy, since such a scan cannot be performed during a wind tunnel test. In the following, frontal areas estimated with tight clothes are used as a proxy for both types of clothes.

2.5 2.5 Test program

The test program is detailed in Table 3. By varying the yaw angle, the dummy positioning, the type of clothes and the presence of a backpack, 83 configurations were considered. In each of them, measurements were conducted for the three wind velocities given in Table 2, leading to a total of 249 experimental tests.

3 Results

The experimental results for the drag area and coefficient are presented in detail in in Sect. 3.1. Results inferred from the experimental observations for the side and lift areas and coefficients are depicted in Sect. 3.2. The observed torques around the vertical axis are discussed in Sect. 3.3. The measured forces are displayed in Figures S4 to S6 in Supplement.

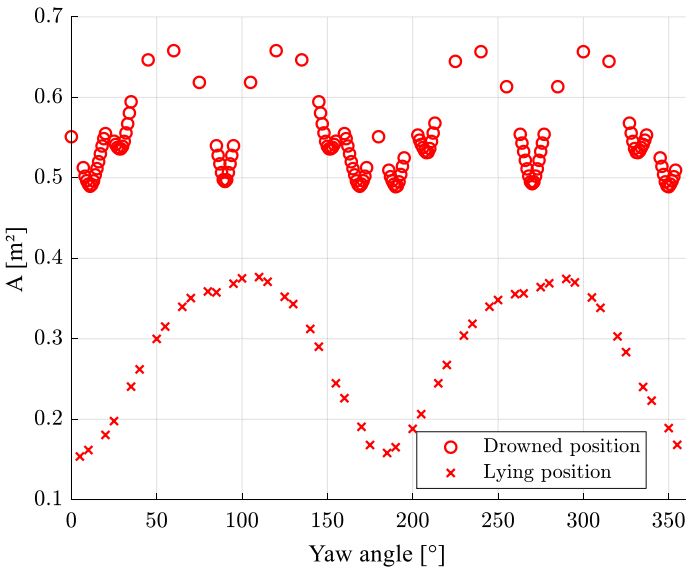

Fig. 5 Frontal area of the dummy in lying and drowned positions in tight clothes, as a function of yaw angle

Table 3 Test program

Yaw angle	Lying position		Drowned position		
	Tight clothes	Loose clothes	Tight clothes	Loose clothes	Loose clothes and backpack
0°	X	X	X	X	X
15°	X	X	X	X	
25°				X	
30°	X	X	X	X	
35°				X	
45°	X	X	X	X	X
60°	X	X	X	X	
75°	X	X	X	X	
90°	X	X	X	X	X
105°			X	X	
120°			X	X	
135°	X	X	X	X	X
145°				X	
150°			X	X	
155°				X	
165°			X	X	
180°	X	X	X	X	X
195°			X	X	
205°				X	
210°			X	X	
225°	X	X	X	X	
240°			X	X	
255°			X	X	
270°	X	X	X	X	
285°			X	X	
300°			X	X	
315°	X	X	X	X	
330°			X	X	
335°				X	
345°			X	X	

All tests were performed for the three wind velocities given in Table 2

3.1 Drag

The evaluated drag areas and coefficients are discussed in the following paragraphs. A summary of the main findings is provided in Table 4. Note that all measured values of the force component F_D fall well above the resolution of the corresponding sensor, as shown in Figure S4 in Supplement. Moreover, in all configurations but four (out of a total of 249, in 98% of the cases), the ratio of the standard deviation of the drag force to the time-averaged value remains below 10% (Figures S29 in Supplement).

Table 4 Outcomes of parameter study for the drag area and coefficient of a human-like body

	Drag area	Drag coefficient
Typical range of variation	0.08–0.65 m^2 (Figs. 6 and 7)	0.5–1.2 (Figs. 10 and 11)
Influence of Reynolds number	Limited: ± 15% (Figure S15 to S17 in Supplement)	Limited: ± 15%
Influence of yaw angle	Lying position: factor 4 to 5 Drowned position: change by no more than 50% (Figs. 6, 7, 8)	Lying position: factor 2 Drowned position: change by no more than 50% (Figs. 10 and 11)
Influence of body position	Median values on all yaw angles change by a factor 2 (Fig. 7) At a yaw angle of 0° or 180°, the difference may reach a factor of 2.5–6 (Figs. 8 and 9a)	No systematic trend (Fig. 12a)
Influence of considering loose clothes instead of tight clothes	+ 20% (Fig. 9b)	Lying position: + 15% Drowned position: + 30% (Figs. 11 and 12)
Influence of adding a backpack	Increase by up to 18% (Fig. 13a)	Increase by up to 18% (Fig. 13b)

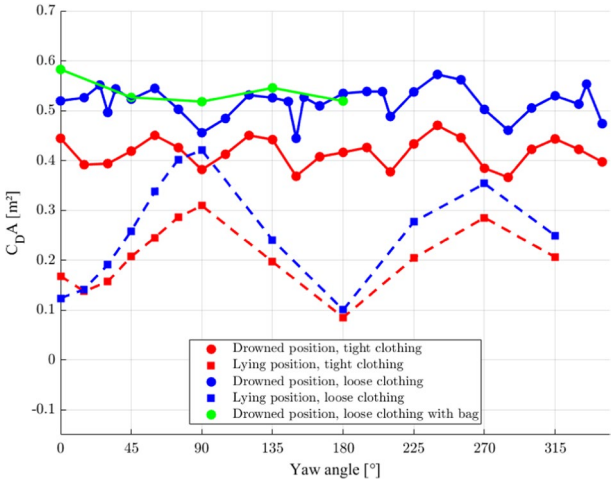

Fig. 6 Drag area as a function of yaw angle in the tested configurations for $\mathrm{Re} = 8.8 \times 10^5$

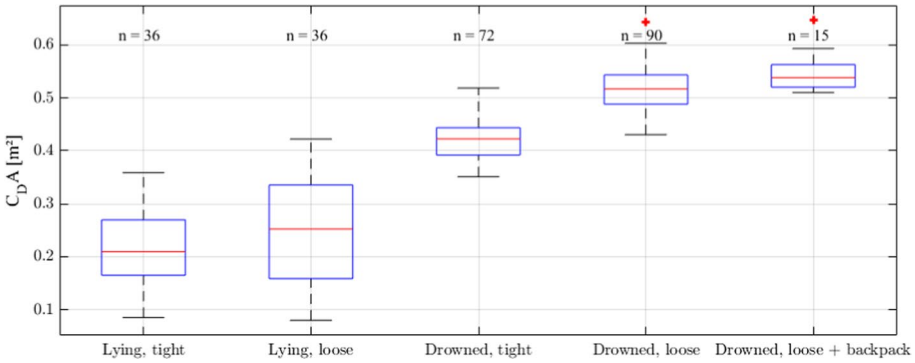

Fig. 7 Boxplots of drag areas for all yaw angles and Reynolds numbers in each configuration (dummy position and type of clothes). For each of them, symbol *n* indicates the number of tests, out of a total of 249, and red crosses represent outliers

3.1.1 Drag area

Figure 6 represents the drag areas evaluated according to Eq. (2), as a function of yaw angle and the configuration (i.e., dummy position, type of clothes, and presence or not of a backpack) for the highest tested Reynolds number. Boxplots in Fig. 7 provide a summary of the measured values of drag area for each configuration. For the sake of readability, Figures S10 to S12 in Supplement show the variation of the drag area as a function of the yaw angle for each individual configuration.

Overall, the observed values of drag area vary in a relatively large range, between 0.09 and 0.59 m^2, which corresponds to almost an order of magnitude of variation (Fig. 6). These variations are mostly explained by the influence of the yaw angle, dummy position, type of clothes, and presence of a backpack. In contrast, the wind velocity (i.e., Reynolds number) shows a limited influence on the drag area (Fig. 8). Regardless of the configuration and the yaw angle, the drag area generally does not vary by more than 15% when the Reynolds number is varied in the range tested here (Figures S15 to S17 in Supplement).

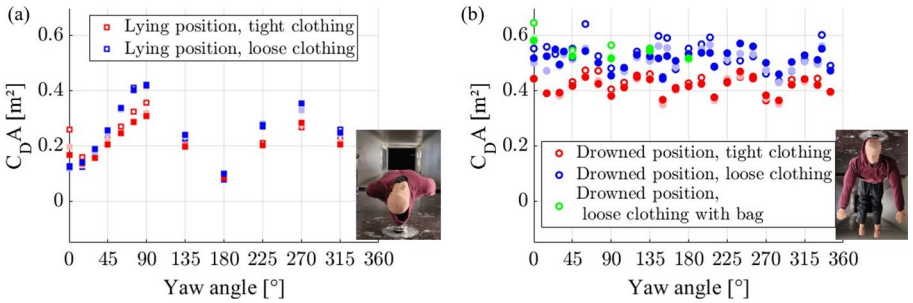

Fig. 8 Drag area as a function of yaw angle in the configurations with loose clothes (**a**) and with tight clothes (**b**). The markers face colour refers to the Reynolds number considered in each test. Empty markers: $Re = 4.3 \times 10^5$, light plain markers: $Re = 6.1 \times 10^5$, and dark plain markers: $Re = 8.8 \times 10.^5$

As shown in Fig. 6, varying the yaw angles has a substantially stronger influence in the case of the lying position than in the drowned position. In the former case, the drag area varies by a factor two (tight clothes) to four (loose clothes) when the yaw angle is changed. In the latter case, the drag area does not vary by more than 50%, irrespective of the type of clothes. This is due to the lower influence of the yaw angle on frontal area in the drowned position than in the lying position.

In the lying position, the drag area varies between 0.08 and 0.42 m^2 (Fig. 7). This range is lower than the range of values observed for the drowned position, which is between 0.35 and 0.52 m^2 with tight clothes, and between 0.43 and 0.64 m^2 with loose clothes (Fig. 9a). The median value of the observed drag areas increases by about a factor two when the dummy position is changed from lying to drowned (Fig. 7). The difference between the two positions is maximum when the yaw angle is 0° or 180°, and minimum when the yaw angle is 90° or 270°. This may be due to differences in the streamwise body length which is maximum for yaw angles of 0° and 180°, and minimum for 90° and 270°. At 0° yaw angle, the drag area can be 2.5 times (tight clothes) to 4 times larger in the drowned position than in the lying one (Figure S18 in Supplement). At a yaw angle of 180°, these factors grow to 4.5 and 6, respectively.

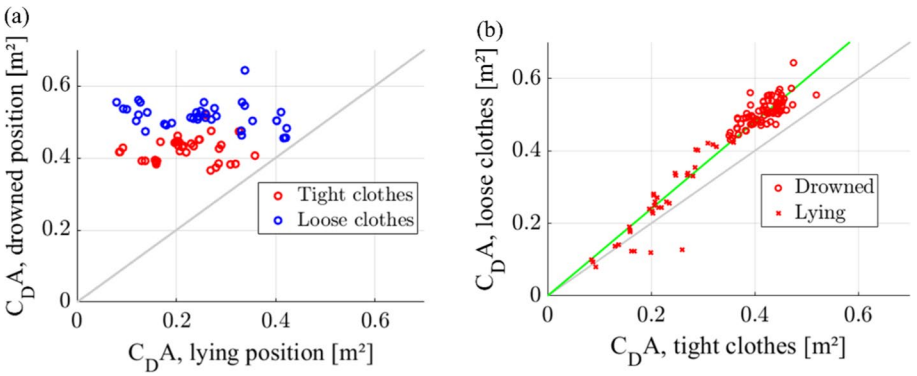

Fig. 9 Influence of **a** the dummy position and **b** the type of clothes on the observed drag areas. The 1:1 line is represented in grey, while the green line follows the slope 1:1.15

Unlike the influence of the yaw angle, the effect of loose or tight clothes is slightly stronger in the drowned position than it is in the lying position. In the latter case, the values are increased by about 15% when loose clothes are used instead of tight ones (with some cases in which these values are decreased), while in the drowned position, the values are magnified by about 20% when loose clothes are used instead of tight ones (Fig. 9b). Adding a backpack further increases the drag area by up to 18% (Fig. 13a).

3.1.2 Drag coefficient

For the highest tested Reynolds number, Fig. 10 represents the drag coefficients evaluated according to Eq. (3), as a function of the yaw angle and the configuration. In Figure S19 to S21 in Supplement, the drag coefficients are also represented for each configuration individually and for all tested Reynolds numbers. Boxplots in Fig. 11 display the variability of the estimated drag coefficient for each configuration.

Compared to the range of variation of the drag area (Fig. 6), the observed values of the drag coefficient vary in a much smaller range (i.e., between 0.5 and 1.2), except for a few outliers (Figs. 10 and 11). Like in the case of the drag area, the influence of the Reynolds number remains small in the tested range (generally less than 15% of variation in the drag coefficient, Figure S19 to S21 in Supplement).

When the yaw angle is systematically varied, the drag coefficient corresponding to the lying position varies between 0.5 and 1.1 (Fig. 11). The ratio of the highest value to the lowest is of the order of two, which is considerably lower than the factor four to five obtained for the drag areas. This ratio is slightly higher in the case of loose clothes than with tight clothes, suggesting that the drag coefficient is more sensitive to the yaw angle for loose clothes than for tight ones. For the drowned position, the variations of the drag coefficient with the yaw angle remain lower than 50%. This is similar to the results obtained for the drag area, as the frontal area shows limited variations with the yaw angle in the case of the drowned position. For the lying position, the variation of the drag coefficient with the yaw angle follows a similar pattern as the corresponding frontal area (Fig. 6), with extrema at comparable yaw angles. For the drowned position, an opposite pattern is observed.

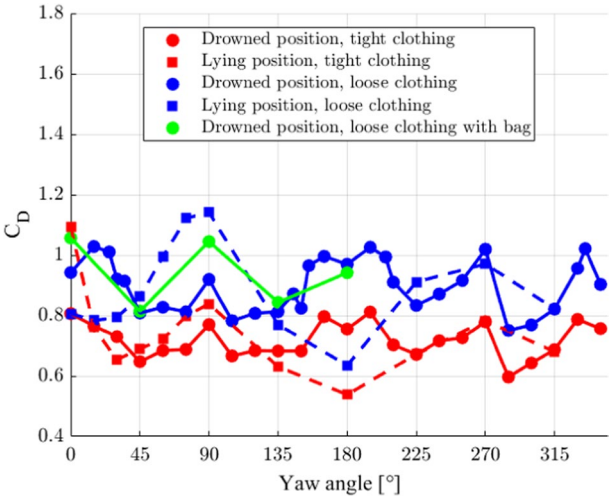

Fig. 10 Drag coefficient as a function of yaw angle in the tested configurations for Re = 8.8 × $10.^5$

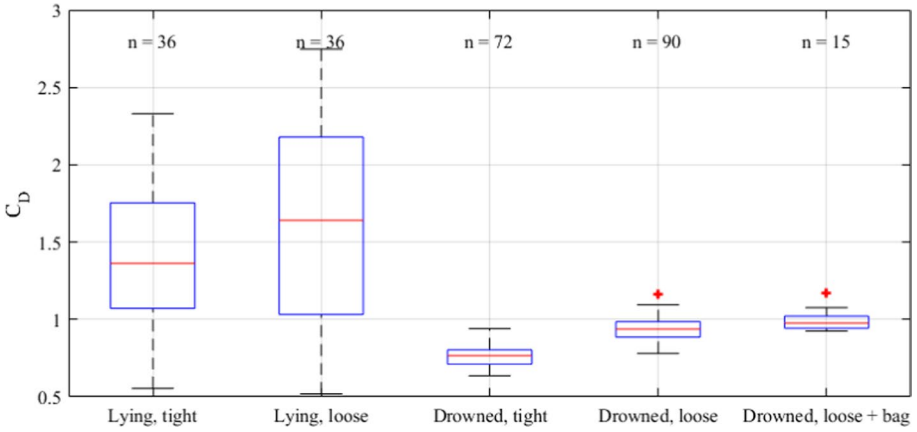

Fig. 11 Boxplots of drag coefficients in each configuration (dummy position and type of clothes)

For each of them, symbol *n* indicates the number of tests, out of a total of 249, and red crosses represent outliers (all at a yaw angle of 0°).

In the lying position, the drag coefficient varies between 0.5 and 0.9 for tight clothes and between 0.5 and 1.2 for loose clothes (Fig. 11). In the drowned position, the ranges are even thinner for both types of clothes (0.6 to 0.9 for tight clothes, and 0.7 to 1.1 for loose clothes). Unlike in the case of the drag areas (Fig. 9a), Fig. 12a reveals that no systematic relation appears between the drag coefficients in drowned and in lying positions. This hints at the capacity of a position-dependent frontal area (Fig. 5) to encompass to a great extent the influence of the dummy position.

Like for the drag areas, the effect of changing the type of clothes is stronger in the drowned position than in the lying position. The mean value of the drag coefficient increases by a about 15% when the type of clothes is changed from tight to loose in the lying position, while this increase reaches 30% for the drowned position (Figs. 11 and 12b).

When a backpack is added in the drowned position (with loose clothes), Figs. 7 and 11 show that the median value is increased by 4% and 3% for the drag area and coefficient, respectively. Such changes are of little significance compared to other effects, such as the

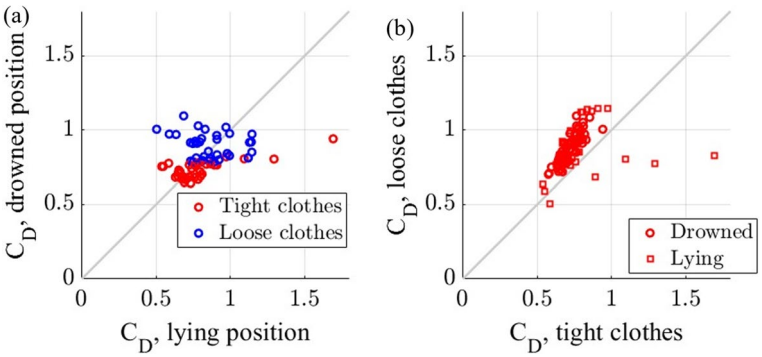

Fig. 12 Influence of **a** the dummy position and **b** the type of clothes on the drag coefficient

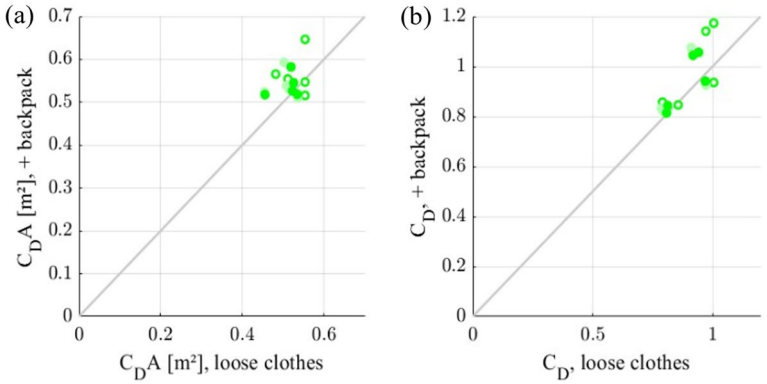

Fig. 13 Influence of the backpack on the **a** drag area and **b** drag coefficient

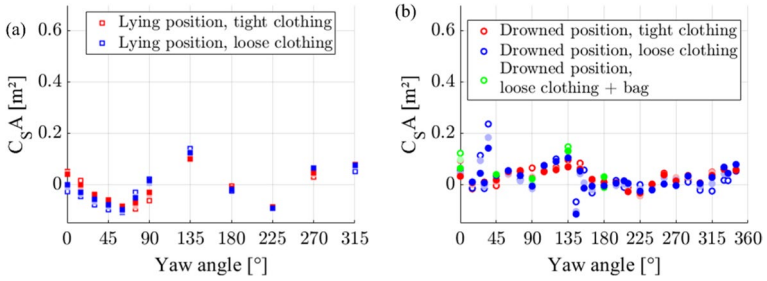

Fig. 14 Side area as a function of yaw angle **a** in the lying position and **b** in the drowned position. The markers face colour refers to the Reynolds number considered in each test. Empty markers: $Re = 4.3 \times 10^5$, light plain markers: $Re = 6.1 \times 10^5$, and dark plain markers: $Re = 8.8 \times 10.^5$

variability induced by changes in the yaw angle. The scatter plots in Fig. 13 reveal that, for a given configuration, an increase in the drag coefficient is not systematic when a backpack is added though it can be as high as 18% in some cases. However, these increases may be partly attributed to an increased frontal A due to the presence of the backpack. This change in the frontal area could not be systematically measured (as in Fig. 5) but it is estimated at maximum 13%.

3.2 Side and Lift

The side area was computed according to Eq. (2). The results are displayed in Fig. 14 for the tested yaw angles, Reynolds numbers and configurations. The yaw angle has a significant influence on the side area, leading to variations ranging mostly from -0.1 m^2 to $+0.15$ m^2 (Fig. 14). This influence is stronger in the lying position than in the drowned position, as shown in Figure S14 in Supplement. A quasi-periodic pattern can be identified in the results of the lying position, with a period of 180° (Fig. 14), whereas visual inspection of Fig. 14b does not reveal a distinctive pattern in the case of the drowned position. Similarly, no systematic trend is observed for the influence of the type of clothes (Figure S22 in Supplement), nor for the effect of adding a backpack

(Figure S23 in Supplement). The absence of trend in some cases may be attributed to the relatively low values of the measured forces, which in a number of configurations are of comparable magnitude as the resolution of the sensor. Figure S5a in Supplement indicates that about 30% of the tested configurations lead to a value of the force component F_S lower than the sensor resolution. The ratio of the standard deviation of the side force to the time-averaged drag force remains below 10% in about 90% of the tested configurations, and the maximum value of this ratio is 25% (Figure S30 in Supplement).

Like for the side area, the side coefficient is less affected by changes in the yaw angle in the case of the drowned position than it is for the lying position (Fig. 15). In the former case, the side coefficient varies between − 0.11 and 0.15, whereas in the latter case it ranges between − 0.35 and 0.4. No significant effect on the side coefficient could be detected when the type of clothes was varied (Figure S22 in Supplement), nor when a backpack was added (Figure S23 in Supplement).

The evaluated lift areas and coefficients are displayed Figure S24 and Figure S25 in Supplement. The lift areas vary between 0 m2 and about 0.2 m2 for the lying position (Figure S24a in Supplement) and between 0 m2 and 0.3 m2 for the drowned position (Figure S24b in Supplement). The lift coefficient varies mostly between 0 and 0.6 irrespective of the considered configuration (Figure S25 in Supplement). In the drowned position, the lift area and coefficients reach a maximum when the yaw angle is close to 180°. Apart from this, the experimental data do not enable detecting any significant pattern, neither when the yaw angle (Figures S24 and S25 in Supplement) or type of clothes (Figure S23 in Supplement) is varied, nor when a backpack is added (Figure S23 in Supplement), which may result from the measured force component F_L being too close to the sensor resolution. Figure S6 in Supplement reveals that, in about 20% of the tested configurations, the value of F_L is lower than the sensor resolution, while issues with the time convergence of this measurement also arise (Figure S3a in Supplement). Moreover, in a quarter of the tested configurations, the standard deviation of the lift force exceeds 10% of the time-averaged drag force, reaching up to about 30% (Figure S3a in Supplement).

The difficulties faced to detect significant trends in the results obtained for the lift area and coefficient, as well as to some extent for the side area and coefficient, may result from limitations in the measurement accuracies. Such difficulties were not encountered in the case of the drag area and coefficient (Sect. 3.1). This may be explained by the

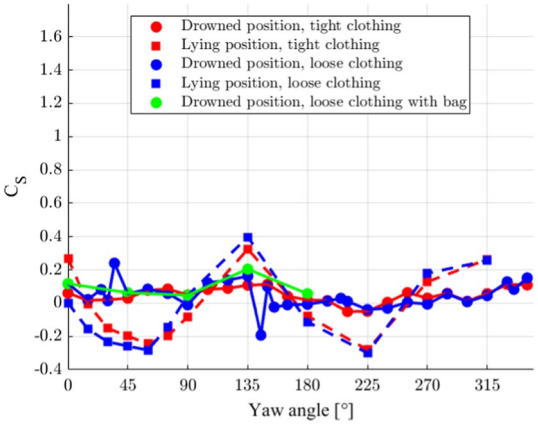

Fig. 15 Side coefficient as a function of yaw angle in the tested configurations for Re = 8.8 × 10^5. Continuous lines are interpolations between the measurements represented by discrete data

relatively lower values of side and lift forces, hence also area and coefficients, compared to the drag, as confirmed in Figure S26 in Supplement.

3.3 Torque in the vertical direction

For the three considered Reynolds numbers, Fig. 16 represents the vertical torques (T_z, also called yawing moments) as a function of yaw angle. Most values of torque lie between -1 Nm and $+1$ Nm. In magnitude, 95% of these measurements are larger than the sensor resolution (Fig. 6b in Supplement). In a few cases, corresponding all to the lying position (and irrespective of the type of clothes), the observed torque values reach -2 Nm or extend up to $+2.8$ Nm. In the drowned position, the torque values range between -0.5 and $+0.5$ Nm with tight clothes, and from -1.2 to 0.9 Nm with loose clothes. These values are strongly dependent on the Reynolds number. Compared to the case of $\mathrm{Re}=4.3\times10^5$, the torque values are about twice higher for $\mathrm{Re}=6.1\times10^5$, and about four times higher for $\mathrm{Re}=8.8\times10^5$, as detailed in Figure S24 in Supplement. Both the body position and the type of clothes also have a substantial influence on the torque values.

The pattern of variation of the torque with the yaw angle differs between the lying and the drowning positions. In the lying position, vertical torques are positive between 0° and 180°, with a maximum value captured around a yaw angle of 75°. The torques become negative for yaw angles 180° and 360°, with a maximum absolute value captured at 270°. In the drowned position, vertical torques are mostly negative between 0° and 180°, though lower in magnitude than in the lying position. They are generally positive for yaw angles between 180° and 360°.

In lying position, the type of clothes has no significant effect on the vertical torque (Fig. 16). In contrast, in the drowned position, extreme values are greater in magnitude in the case of loose clothes than with tight clothes and torques are strictly positive for yaw angles over 180° with loose clothes. Adding a backpack does not lead to any significant difference in torques compared to the same configurations without backpack.

The observed torque values suggest that different equilibria exist depending on the body position. In the lying position, equilibrium at $\theta=0°$ is unstable. Indeed, if the body deviates slightly, say towards positive values of the yaw angle, a positive moment acts on the body which makes it rotate further and leave its initial equilibrium position. Vice-versa, equilibrium with a yaw angle of $\theta=180°$ is stable, as slight variations in the yaw angle around $\theta=180°$ induce moments which tend to shift back the body to its equilibrium position at $\theta=180°$. For the drowned, the opposite is found: the equilibrium at $\theta=0°$ is stable, while the equilibrium at $\theta=180°$ is unstable. Consequently, depending on the body position (lying or drowned), the body tends to align with the flow with the head located either upwind (lying position) or downwind (drowning position).

4 Discussion

4.1 Comparison with standard shapes

Drag coefficients are influenced by multiple parameters, including Reynolds number, wall roughness, turbulence intensity, shear in approach flow, proximity of a wall, and interactions between multiple obstacles (Achenbach 1974; Dubois and Andrianne 2022). Here, for setting in perspective the drag coefficients obtained for novel configurations (human

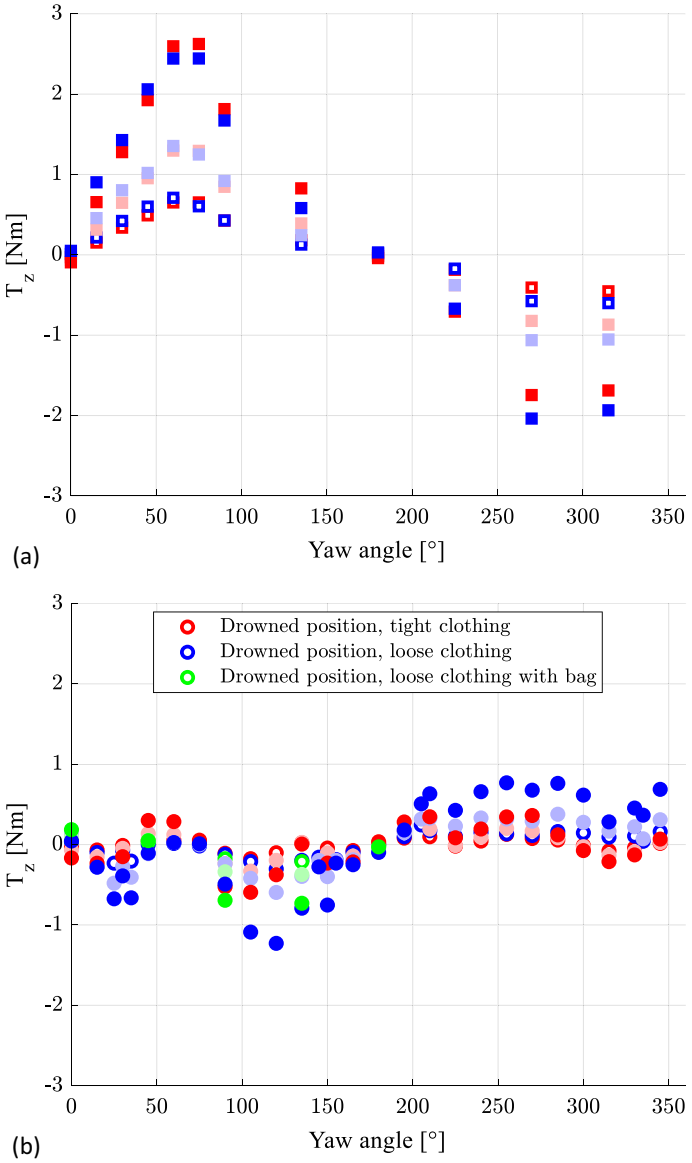

Fig. 16 Vertical torque as a function of yaw angle **a** for the lying position and **b** for the drowned position. The markers face colour refers to the Reynolds number considered in each test. Empty markers: $Re = 4.3 \times 10^5$, light plain markers: $Re = 6.1 \times 10^5$, and dark plain markers: $Re = 8.8 \times 10.^5$

body in drowning position, with various clothes types and body orientations with respect to the approach flow), they are compared to a few well-known reference configurations, without systematically exploring the effect of all possible influencing parameters on the reference cases.

In Fig. 17, the ranges of variation of the drag coefficient derived from our experimental observations are compared to values characterizing two reference shapes: a smooth sphere

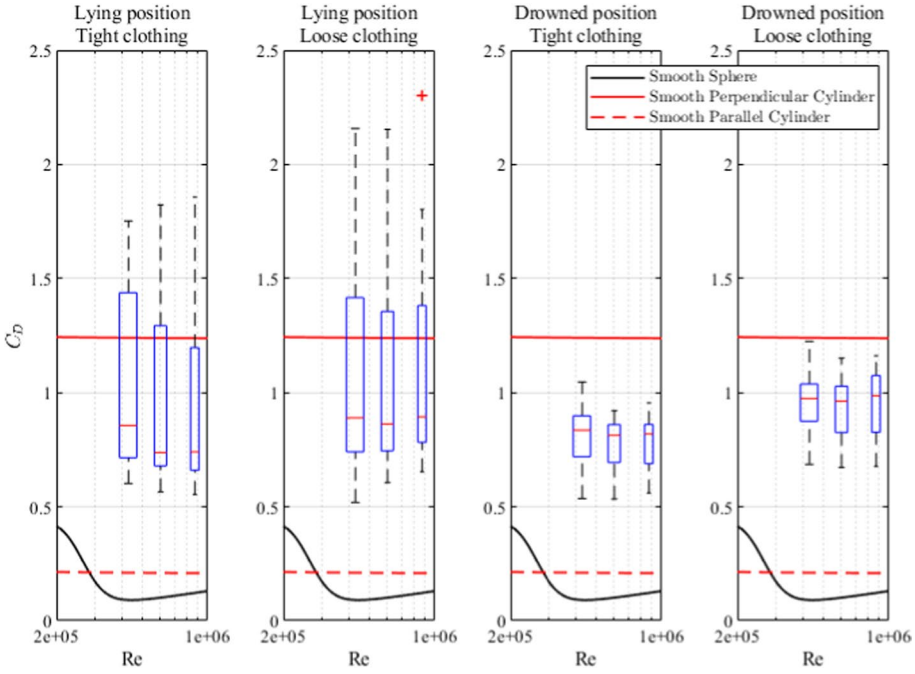

Fig. 17 Estimated drag coefficient as a function of the Reynolds number, for each configuration (body position and type of clothes), with boxplots reflecting the variability of the drag coefficient with the yaw angle. Comparison with reference values for a smooth sphere (Morrison 2013) and smooth cylinders, either aligned with (i.e., parallel to) or normal (i.e., perpendicular) to the approach flow (Hölzer and Sommerfeld 2008)

(Morrison 2013), and a smooth cylinder of radius 0.2 m and of finite length equal to 1.9 m, with its axis either aligned with or normal to the approach flow (Hölzer and Sommerfeld 2008). To estimate the drag coefficient of smooth cylinders and spheres, Hölzer and Sommerfeld (2008) and Morrison (2013) used data from experiments conducted both with air and with water. They systematically applied Reynolds similarity to combine data originating from tests carried out with different fluids (Roos and Willmarth 1971). This relatively standard procedure of using Reynolds similarity for transferring results obtained with one fluid to another one also supports our approach consisting in performing tests with air (wind tunnel) and transfer the outcomes to water (rivers).

For each tested configuration (body position and type of clothes), Fig. 17 represents the drag coefficient as a function of the Reynolds number, using boxplots to reflect the variability of the coefficient with the yaw angle.

Compared to the variability of the drag coefficients with the yaw angle, the drag coefficients evaluated here hardly vary with the Reynolds number in the tested range. In the case of a sphere, variations are visible in Fig. 17 due to the drag crisis occurring in this range of Reynolds number. For the cylinders the considered range of Reynolds number is below the range corresponding to the drag crisis.

The relative positioning of our experimental results compared to the reference values appears reasonable, both in terms of extent of the influence of the yaw angle and in terms of absolute values.

4.1.1 Influence of yaw angle

The difference between the drag coefficients of cylinders with axis normal (i.e., perpendicular) to the approach flow (i.e., yaw angle of 90° or 270°, $C_D = 1.24$) and aligned with the approach flow (i.e., yaw angle of 0° or 180°, $C_D = 0.21$) is of the order of 1. This is similar to the extent of the variation of the drag coefficients (as represented by the boxplots) when the yaw angle is varied for the dummy in lying position. The cylinder used by Hölzer and Sommerfeld (2008) may be seen as a highly idealized version of the dummy, leading to comparable changes in the drag coefficient when the yaw angle is varied. Figure 10 shows that the drag coefficient is maximum when the yaw angle is 90° or 270° (similar to the cylinder normal to the approach flow) and minimum when the yaw angle is 0° or 180° (similar to the cylinder aligned with the flow).

When the yaw angle is varied, the changes in the values of the drag coefficient of the dummy in drowned position are considerably lower than the difference between the drag coefficients of the cylinders normal to the approach flow and aligned with the approach flow. This is due to the more compact shape of the drowned positioning compared to a cylinder.

4.1.2 Absolute values

Despite some similarity between the body in lying position and cylinders, the drag coefficients found for the body in lying position are above those of cylinders. The lowest values of the drag coefficients estimated here are around 0.5 (corresponding to yaw angles of 0° or 180°, as shown in Fig. 10), which is about 2.5 times greater than the corresponding values for a cylinder with its axis aligned with the approach flow (Fig. 17). This is because a cylinder is a more streamlined shape than a human-like body. For the same reason, the highest values of the drag coefficients found for the dummy in lying position (corresponding to yaw angles of 90° or 270°, as shown in Fig. 10) are also above the values characterizing a cylinder with axis normal to the flow, i.e. with the same yaw angle.

Drag coefficients obtained for the body in drowned position lie in-between the case of a cylinder with axis aligned with the approach flow and that of a cylinder with axis normal to the approach flow. Irrespective of the body positioning, the drag coefficients obtained for a human-like body are at least four times larger than the value characterizing a sphere ($C_D \sim 0.1$) in the same range of Reynolds number.

4.1.3 Reynolds dependency

In the considered range of Re, the drag coefficient of a sphere varies between 0.4 and 0.15 due to the drag crisis while this coefficient is equal to 0.21 for a cylinder aligned with the flow and 1.24 for a finite cylinder perpendicular to the flow. Figure 18 shows no drag crisis in the case of a human body and no clear influence of the Reynolds number on the values of drag coefficient in the tested range of Reynolds number. These observations are not affected by the choice of a particular characteristic length in the definition of the Reynolds number (e.g., body height vs. trunk height for the drowning position).

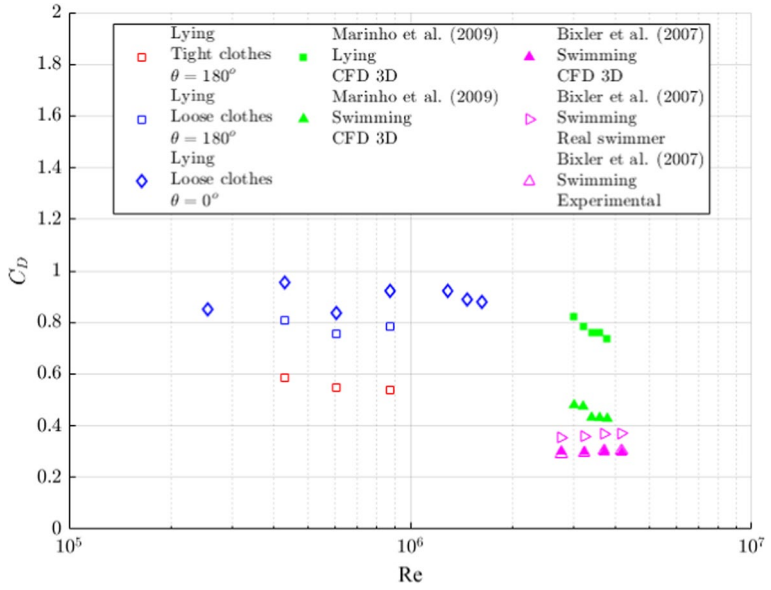

Fig. 18 Comparison between this study and previous studies focused on body in swimming position, based either on experiments with a real swimmer or a dummy, or on computational fluid dynamics (CFD). Square and diamond markers refer to the lying position described in Sect. 2.2, while triangle markers correspond to swimming position (lying position with arms aligned in the front of the head)

4.2 Comparison with studies on swimming

The drag coefficient characterizing a human body has been studied for a variety of settings, including positions corresponding to swimming (Bixler et al. 2007; Marinho et al. 2009, 2011, 2012; Zamparo et al. 2009; Mantha et al. 2014), ice skating (Ingen Schenau 1982), ski jumping (Müller 2009; Wolfsperger et al. 2021), speed skiing (Barelle et al. 2004), cycling (García-López et al. 2008), standing, sitting or supine positions (Schmitt 1954). Although most of these positions differ substantially from the drowned and lying positions of interest here, the swimming position shows some similarities with the lying position considered here when the head is oriented towards upwind. In Fig. 18, we compare our results in lying position with a yaw angle of 180° and tight clothes and a yaw angle of 0° and 180° for loose clothes against values of drag coefficient reported in literature for swimmers (Bixler et al. 2007; Marinho et al. 2009). Measurements in lying position with a yaw angle of 0° and tight clothes are considered as inconsistent. Indeed, these values fail to agree with the pattern observed in C_D as a function of the yaw angle in all other considered configurations (see Fig. 28 in Supplement). The range of Reynolds number tested here is about five times lower than the ranges considered by Bixler et al. (2007) and Marinho et al. (2009), and it is consistent with what could be observed in a river.

Bixler et al. (2007) performed flume tests with a dummy and with a real swimmer, as well as simulations using a 3D computational fluid dynamics (CFD) model. A body positioning typical of swimming was considered, with the limbs aligned with the trunk and arms in front of the head. In each case, the body was positioned at a distance of

0.75 m from the free surface, so that the surface had no significant effect when bodies are at such a depth (Vennell et al. 2006). They found a remarkable agreement between their experimental observations with a dummy and their computations, leading to a drag coefficient of about 0.3. A slightly higher value was obtained in the tests conducted with a real swimmer ($C_D \approx 0.36$).

The results of Marinho et al. (2009) are solely based on computations. Though the 3D simulations of Marinho et al. (2009) consider the same body positioning as Bixler et al. (2007) but at a depth of 2 m, they lead to a drag coefficient about 50% higher than in the experimental data of Bixler et al. (2007). They found that the drag coefficient in lying position is about 75% higher than in gliding position. The experimental data of Bixler et al. (2007) are 80% lower than the values of our tests with the dummy in lying position at a yaw angle of 180° and tight clothes. This is consistent with the less streamlined nature of the lying position compared to the swimming one with arms in front of the head. Marinho et al. (2009) estimate this effect at about 75% higher, which matches fairly well the value of 80% obtained by comparing the present tests to those of Bixler et al. (2007).

5 Conclusion

Full scale experimental tests have been conducted with a dummy in a wind tunnel to evaluate hydrodynamic coefficients of interest for reproducing the effect of drag, side and lift forces in a computational model of the drift of a victim of drowning. The experimental results are presented (i) in terms of drag, side and lift areas, which are independent of a particular estimation of the frontal area but are not transferrable across scales, and (ii) in terms of drag, lift, and side coefficients. In the conducted laboratory tests, the wind velocity ($\mathrm{Re} = 4.3 \times 10^5$ to 8.8×10^5), the yaw angle, the type of clothes (tight vs. loose), and the body position (lying vs. typical position of a victim of drowning) were systematically varied. The following observations could be made:

- Both the drag coefficient and the drag area change by maximum 15% when the Reynolds number is varied in the tested range.
- Changing the yaw angle has a considerably stronger influence on the drag area for a body in lying position than when it is in the typical position of a drowning victim, which is more compact. In the former case, the maximum and minimum drag areas differ by a factor two (with tight clothes) to four (with loose clothes) when the yaw angle is varied, while in the latter case the drag area does not change by more than 50%.
- For a body in lying position, the drag coefficient tends to be less influenced by the yaw angle than the drag area, as the minimum ($C_D \approx 0.5$) and maximum ($C_D \approx 1$) values of the drag coefficient differ by a factor two. In the drowned position, changing the yaw angle induces variations in the drag coefficient ($C_D \approx 0.6$ to 1) of approximately 50%, like for the drag area.
- While the drag area differs substantially between a body lying position and in drowned position, no distinctive effect of the body position could be detected for the drag coefficient.
- Compared to the case of a body equipped with tight clothes, the drag area for a body with loose clothes is about 20% higher, while the drag coefficient is increased by 15% (lying position) and 30% (drowned position).

- Adding a backpack does not systematically alter the drag area and coefficient; but in several configurations it induces an increase by up to 20%.

The measured side and lift forces are generally lower than the corresponding drag force for the same configuration and wind velocity. Since the measured side and lift forces are in many cases comparable to the sensitivity of the sensors, it was difficult to detect distinctive trends in the side and lift coefficients when the yaw angle, type of clothes or body position were varied. It could nonetheless be observed that the side coefficient is less affected by changes in the yaw angle in the case of the drowned position (variations between -0.11 and 0.24) than it is for the lying position, (variations between -0.35 and 0.5).

The present study has a number of limitations, as detailed hereafter.

- While the available experimental setup enabled a systematic exploration of the influence of body orientation and position, only a relatively narrow range of Reynolds numbers could be tested. Hence, future research should aim at further analysing the influence of the Reynolds number on the hydrodynamic coefficients of a human-like body in drowned position.
- Similarly, the effect of turbulence intensity in the approach flow and the influence of the distance to the wall need further investigations since these parameters remained fixed in the present series of tests.
- It is also necessary to study the force coefficients in configurations in which the flow velocity varies over the height of the body, as typically observed in shear flow in rivers, since the velocity profile has an influence on the hydrodynamic forces.
- Since our data were obtained solely based on a dummy reproducing a male adult individual, future research should assess the validity of our results when transferred to the case of a female adult or a child.
- The influence of the free surface on the force coefficients could not be captured in the present series of tests, while they are not negligible when the distance from the body to the surface is relatively low (e.g., below 0.75 m according to Vennell et al. (2006) for the case of swimmers). This specific aspect should be analysed in future experiments based on a towing or a current flume.

Finally, the scope of the research should be extended towards more reliable assessment of the side and lift coefficient (e.g., using more sensitive sensors along the corresponding direction than for monitoring the drag force), and towards the evaluation of other parameters critical for drift modelling such as the added mass coefficient.

Supplementary Information The online version contains supplementary material available at https://doi.org/10.1007/s11069-024-06498-0.

Acknowledgements The authors thank Dr. Raphael Dubois for his support and expertise in the use of the wind tunnel and its equipment.

Author contributions All authors contributed to the study conception and design. Material preparation, data collection and analysis were performed by Clément Delhez, Benjamin Dewals and Thomas Andrianne. The first draft of the manuscript was written by Clément Delhez and all authors commented on previous versions of the manuscript. All authors read and approved the final manuscript.

Funding The authors declare that no funds, grants, or other support were received during the preparation of this manuscript.

Declarations

Conflict of interest The authors have no relevant financial or non-financial interests to disclose.

References

Achenbach E (1974) The effects of surface roughness and tunnel blockage on the flow past spheres. J Fluid Mech 65:113–125

Amendt J, Krettek R, Zehner R (2004) Forensic entomology. Naturwissenschaften 91:51–65

Anderson J (2011) Fundamentals of aerodynamics, 5th edn. McGraw-Hill, NewYork

Barelle C, Ruby A, Tavernier M (2004) Experimental model of the aerodynamic drag coefficient in alpine skiing. J Appl Biomech 20:167–176

Barwood MJ, Bates V, Long G, Tipton MJ (2011) Float First:" trapped air between clothing layers significantly improves buoyancy on water after immersion. Int J Aquat Res Educ 5:3

Bierens JJLM (ed) (2006) Handbook on drowning: prevention, rescue, treatment. Springer, Berlin

Bixler B, Pease D, Fairhurst F (2007) The accuracy of computational fluid dynamics analysis of the passive drag of a male swimmer. Sports Biomech 6:81–98

Blocken B, van Druenen T, Toparlar Y, Andrianne T (2018) Aerodynamic analysis of different cyclist hill descent positions. J Wind Eng Ind Aerodyn 181:27–45

Blondel P (2014) Searching for dead bodies with sonar. Drowning prevention, rescue treatment. Springer-Verlag, Berlin, pp 1161–1165

Breivik Ø, Allen AA (2008) An operational search and rescue model for the Norwegian Sea and the North Sea. J Mar Syst 69:99–113

Byard RW (2017) Drowning deaths in rivers. Forensic Sci Med Pathol 13:388–389

Carniel S, Umgiesser G, Sclavo M, Kantha LH, Monti S (2002) Tracking the drift of a human body in the coastal ocean using numerical prediction models of the oceanic, atmospheric and wave conditions. Sci Justice: J Forensic Sci Soc 42:143–151

Cook MV (2007) Flight dynamics principles: a linear systems approach to aircraft stability and control. Elsevier aerospace engineering series, 2nd edn. Butterworth-Heinemann/Elsevier, Oxford

Delhez C, Rivière N, Erpicum S, Pirotton M, Archambeau P, Arnst M, Bierens J, Dewals B (2023) Drift of a drowning victim in rivers: conceptualization and global sensitivity analysis under idealized flow conditions. Water Resour Res 59:e2022WR034358

Donoghue ER, Minnigerode SC (1977) Human body buoyancy: a study of 98 men. J Forensic Sci 22:573–579

Du Bois D, Du Bois EF (1989) A formula to estimate the approximate surface area if height and weight be known. 1916. Nutrition (Burbank, Los Angeles County, Calif.) 5:303–311

Dubois R, Andrianne T (2022) Flow around tandem rough cylinders: effects of spacing and flow regimes. J Fluids Struct 109:103465

Gallagher D, Visser M, Sepulveda D, Pierson RN, Harris T, Heymsfield SB (1996) How useful is body mass index for comparison of body fatness across age, sex, and ethnic groups? Am J Epidemiol 143:228–239

García-López J, Rodríguez-Marroyo JA, Juneau C-E, Peleteiro J, Martínez AC, Villa JG (2008) Reference values and improvement of aerodynamic drag in professional cyclists. J Sports Sci 26:277–286

Ghaffarian H, Lopez D, Mignot E, Piegay H, Riviere N (2020) Dynamics of floating objects at high particulate Reynolds numbers. Phys Rev Fluids 5:054307

Gonzalez JRP, Escobar-Vargas J, Vargas-Luna A, Castiblanco S, Trujillo D, Guatame AC, Corzo G, Santos G, Perez LA (2022) Hydroinformatics tools and their potential in the search for missing persons in rivers. Forensic Sci Int 341:111478

Gunduz M (2017) Possible recovery site of four non-recovered bodies lost in the Marmara Sea by using an ocean circulation model. Aust J Forensic Sci 49:154–160

Hart-Davis MG, Backeberg BC (2023) Towards a particle trajectory modelling approach in support of South African search and rescue operations at sea. J Op Oceanogr 16:131–139

Hoerner S (1965) Fluid-dynamic drag: practical information on aerodynamic drag and hydrodynamic resistance, 2nd edn. Cambridge University Press, Brick Town

Hölzer A, Sommerfeld M (2008) New simple correlation formula for the drag coefficient of non-spherical particles. Powder Technol 184:361–365

Jonkman S, Penning-Rowsell, E., (2008) Human instability in flood flows. JAWRA J Am Water Resour Assoc 44:1208–1218

Kringsholm B, Jakobsen J, Sejrsen B, Gregersen M (2001) Unidentified bodies/skulls found in danish waters in the period 1992–1996. Forensic Sci Int 123:150–158
Laurent P-E, Coulange M, Bartoli C, Boussuges A, Rostain J-C, Luciano M, Cohen F, Rolland P-H, Mancini J, Piercecchi M-D, Vidal V, Gorincour G (2013) Appearance of gas collections after scuba diving death: a computed tomography study in a porcine model. Int J Legal Med 127:177–184
Ličer M, Estival S, Reyes-Suarez C, Deponte D, Fettich A (2020) Lagrangian modelling of a person lost at sea during the Adriatic scirocco storm of 29 October 2018. Nat Hazard 20:2335–2349
Lunetta P, Ebbesmeyer C, Molenaar J (2014) Behaviour of dead bodies in water. Drowning. Springer-Verlag, Berlin, pp 1149–1152
Mannion P, Toparlar Y, Clifford E, Hajdukiewicz M, Andrianne T, Blocken B (2019) The impact of arm-crank position on the drag of a paralympic hand-cyclist. Comput Methods Biomech Biomed Eng 22:386–395
Mantha VR, Marinho DA, Silva AJ, Rouboa AI (2014) The 3D CFD study of gliding swimmer on passive hydrodynamics drag. Braz Arch Biol Technol 57:302–308
Marinho DA, Reis VM, Alves FB, Vilas-Boas JP, Machado L, Silva AJ, Rouboa AI (2009) Hydrodynamic drag during gliding in swimming. J Appl Biomech 25:253–257
Marinho D, Barbosa T, Rouboa A, Silva A (2011) The Hydrodynamic study of the swimming gliding: a two-dimensional computational fluid dynamics (CFD) analysis. J Hum Kinet 29:49–57
Marinho DA, Mantha VR, Vilas-Boas JP, Ramos RJ, Machado L, Rouboa AI, Silva AJ (2012) Effect of wearing a swimsuit on hydrodynamic drag of swimmer. Braz Arch Biol Technol 55:851–856
Martlin BA, Anderson GS, Bell LS (2023) A review of human decomposition in marine environments. Can Soc Forensic Sci J 56:92–121
Mateus M, de Pablo H, Vaz N (2013) An investigation on body displacement after two drowning accidents. Forensic Sci Int 229:6–12
Mateus M, Pinto L, Chambel-Leitão P (2015) Evaluating the predictive skills of ocean circulation models in tracking the drift of a human body: a case study. Aust J Forensic Sci 47:322–331
Mateus M, Canelas R, Pinto L, Vaz N (2020) When tragedy strikes: potential contributions from ocean observation to search and rescue operations after drowning accidents. Front Mar Sci 7:55
Modell JH, Davis JH (1969) Electrolyte changes in human drowning victims. Anesthesiology 30:414–420
Morrison FA (2013) An introduction to fluid mechanics. Cambridge University Press, Cambridge
Mosteller RD (1987) Simplified calculation of body-surface area. N Engl J Med 317:1098
Müller W (2009) Determinants of ski-jump performance and implications for health. Safety Fairness Sports Med 39:85–106
Pampín JB Rodríguez BA (2001) Surprising drifting of bodies along the coast of Portugal and Spain. Legal Med 3:177–182
Parks RM, Bennett JE, Tamura-Wicks H, Kontis V, Toumi R, Danaei G, Ezzati M (2020) Anomalously warm temperatures are associated with increased injury deaths. Nat Med 26:65–70
Roos FW, Willmarth WW (1971) Some experimental results on sphere and disk drag. AIAA J 9:285–291
Ruffell A, Pringle JK, Cassella JP, Morgan RM, Ferguson M, Heaton VG, Hope C, McKinley JM (2017) The use of geoscience methods for aquatic forensic searches. Earth Sci Rev 171:323–337
Schmitt TJ (1954) Wind-tunnel investigation of air loads on human beings. U.S. Navy, David W. Taylor Model Basin, Aerodynamics Laboratory.
Strom MA, Pasternack GB, Burman SG, Dahlke HE, Sandoval-Solis S (2017) Hydraulic hazard exposure of humans swept away in a whitewater river. Nat Hazards 88:473–502
Tikuisis P, Meunier P, Jubenville C (2001) Human body surface area: measurement and prediction using three dimensional body scans. Eur J Appl Physiol 85:264–271
Tropea C, Yarin AL, Foss JF (eds) (2007) Springer handbook of experimental fluid mechanics. Springer, Berlin
Tu H, Wang X, Mu L, Xia K (2021) Predicting drift characteristics of persons-in-the-water in the South China Sea. Ocean Eng 242:110134
Ung, A., Gautier, A., Chatignoux, É., Beltze, N., 2019. Main results of the NOYADES survey carried out during summer 2018 in France. Bulletin épidémiologique hebdomadaire 286–94.
Van Hoyweghen AJL, Jacobs W, Beeck BO, de, Parizel, P.M., (2015) Can post-mortem CT reliably distinguish between drowning and non-drowning asphyxiation? Int J Legal Med 129:159–164
van Ingen Schenau GJ (1982) The influence of air friction in speed skating. J Biomech 15:449–458
Vennell R, Pease D, Wilson B (2006) Wave drag on human swimmers. J Biomech 39:664–671
WHO, 2014. Global report on drowning: preventing a leading killer.
Wolfsperger F, Meyer F, Gilgien M (2021) Towards more valid simulations of slopestyle and big air jumps: aerodynamics during in-run and flight phase. J Sci Med Sport 24:1082–1087

Wu J, Cheng L, Chu S (2023) Modeling the leeway drift characteristics of persons-in-water at a sea-area scale in the seas of China. Ocean Eng 270:113444

Yu C-Y, Lin C-H, Yang Y-H (2010) Human body surface area database and estimation formula. Burns 36:616–629

Zamparo P, Gatta G, Pendergast D, Capelli C (2009) Active and passive drag: the role of trunk incline. Eur J Appl Physiol 106:195–205